HHS Public Access

Author manuscript

Cell Rep. Author manuscript; available in PMC 2016 June 13.

Published in final edited form as:

Cell Rep. 2016 February 16; 14(6): 1477–1487. doi:10.1016/j.celrep.2015.12.105.

Drosophila Lung Cancer Models Identify Trametinib Plus Statin as Candidate Therapeutic

Benjamin D. Levine and **Ross L. Cagan**

Department of Developmental and Regenerative Biology *and* the Graduate School of Biomedical Sciences; Icahn School of Medicine at Mount Sinai; One Gustave Levy Place; New York, NY 10029-1020

Summary

We have developed a Drosophila lung cancer model by targeting $Ras1^{G12V}$—alone or in combination with PTEN knockdown—to the Drosophila tracheal system. This led to overproliferation of tracheal tissue, formation of tumor-like growths, and animal lethality. Screening a library of FDA approved drugs identified several that improved overall animal survival. We explored two hits: the MEK inhibitor trametinib and the HMG-CoA reductase inhibitor fluvastatin. Oral administration of these drugs inhibited Ras and PI3K pathway activity, respectively; in addition, fluvastatin inhibited protein prenylation downstream of HMG-CoA reductase to promote survival. Combining drugs led to synergistic suppression of tumor formation and rescue lethality; similar synergy was observed in human A549 lung adenocarcinoma cells. Notably, fluvastatin acted both within transformed cells and also to reduce whole body trametinib toxicity in flies. Our work supports and provides further context for exploring the potential of combining statins with MAPK inhibitors such as trametinib to improve overall therapeutic index.

Keywords

Drosophila; non-small cell lung cancer; trametinib; fluvastatin; trachea

Introduction

Lung cancer is the leading cause of cancer-related mortality worldwide with non-small cell lung cancer (NSCLC) accounting for 85% of disease diagnoses. Standard of care commonly includes a targeted therapy combined with chemoradiotherapy; multiple targeted therapies are currently approved for use in NSCLC. These drugs provide important first- and second-line therapies. In many patients, however, these drugs have shown limited success in suppressing tumor progression due to limited efficacy, emergent resistance, and significant

Correspondence to: Ross L. Cagan.

Author Contributions

Conceptualization, Methodology, Writing, B.L. and R.C; Investigation, B.L.; Funding Acquisition, Supervision, R.C.

toxicity. As a result, NSCLC continues to represent a significant unmet clinical need. Current efforts to identify new drugs and drug cocktails would benefit from whole animal approaches that account for complex and often unpredictable drug activities. Here we present a Drosophila model of lung cancer as a platform to identify and explore candidate therapeutics.

A number of publications have highlighted the similarities between Drosophila tracheal and vertebrate lung development (Roeder et al. 2012; Behr 2010; Andrew and Ewald 2010). The Drosophila tracheal system is an extensively branched tubular network that supplies oxygen to the fly. Both vertebrate lung and Drosophila tracheal systems are formed from an interconnected tubular hierarchy that begin in large primary tubes and branch into diminishing diameter segments that end in terminal branches. During Drosophila tracheal development the branching process is highly dependent on FGF (Fibroblast Growth Factor) signaling. Tracheal cells express the FGF receptor homolog Breathless (Btl), which responds to localized presence of the FGF ligand Branchless to initiate branching. Vertebrate lung development relies on FGF signaling in a similar manner during airway branching (Park et al. 1998; Bellusci et al. 1997).

Here we present the results of tracheal-targeted expression of the oncogenic isoform $Ras1^{G12V}$ plus knockdown of the PI3K negative regulator PTEN. Activated Ras isoforms represent the most common genetic mutations associated with NSCLC, and are typically associated with activated PI3K pathway signaling (Kandoth et al. 2013; Cancer Genome Atlas Research Network 2012). Screening a library of FDA approved compounds yielded multiple hits including the MEK inhibitor trametinib and the HMG-CoA reductase inhibitor fluvastatin. We provide evidence that these two drugs act synergistically to reduce the effects of Ras/PI3K pathway activation. The result is improved tracheal development, reduced overproliferation, and reduced whole animal toxicity; the two drugs also acted synergistically to suppress growth in a standard human lung cancer cell line. We demonstrate that fluvastatin acts through multiple targets to improve overall efficacy, and our data suggests that fluvastatin may prove useful to reduce the whole body toxicity profiles that are common to targeted therapies.

Results

Drosophila lung cancer model

To reliably manipulate gene sets we built vectors containing multiple UAS-elements using a ‘repeat ligation method’ (Fig. 1A; see Experimental Procedures). With this reiterative cloning approach we created Drosophila lines with transgenes inserted into the same attP insertion site to ensure comparable expression levels. The resulting lines expressed transgenes that directed expression of the oncogenic Ras1 isoform $Ras1^{G12V}$ and/or RNA interference-mediated knockdown of the PI3K pathway inhibitor PTEN (*PTENi*), addressing two pathways commonly activated in NSCLC patients (Kandoth et al. 2013; Cancer Genome Atlas Research Network 2012). To express these transgenes within the Drosophila trachea we added the driver *breathless-gal4* (*btl-GAL4*) by standard genetic crosses. *btl-Gal4* is expressed primarily in the trachea; expression is also reported in midline glia within the ventral nerve cord (Shiga et al 1996). The result was establishment of four lines: *btl>control,*

btl>Ras1, btl>PTENi and *btl>Ras1,PTENi*. The full genotypes are listed in Fig. 1A; all include expression of the visible marker green fluorescent protein (GFP) to visualize transformed cells.

The transgenic line *btl>control* directed GFP expression primarily within tracheal tissue throughout development including the L3 larval stage, confirming specificity of the driver (Fig. 1B). *btl>Ras1,PTENi* L3 larvae exhibited tracheal tubes with thicker walls than control animals, likely due to a significant increase in nuclear size typical of transformed cells (Fig. 1C; Fig. S1). In addition, *btl>Ras1,PTENi* L3 larval tracheal tubes tended towards increased width (not significant; Fig.S1) and exhibited fine terminal branching (Fig. 1C). The result was a lethal phenotype: at 25°C, *btl>Ras1* and *btl>Ras1,PTENi* survived to pharate (late pupal) stage but exhibited low levels of eclosion to adulthood. At 29°C—a temperature at which the *btl-GAL4* driver is more active—both lines died during early larval (L1-L2) stages; *btl>PTENi* —lacking $Ras1^{G12V}$—showed no detectable phenotype (data not shown). While we anticipate that lethality is due to tracheal expression, we cannot rule out a contribution by *btl-GAL4*'s midline expression.

Screen for candidate therapeutics

btl>Ras1,PTENi animals die as larvae at 29°C. Using a robotics-based screening approach and a 96-well format (see Experimental Procedures), we screened a library of 1192 FDA approved drugs for drugs that rescued animals to pupariation (Fig. 2A). Hits were subsequently tested in *btl>Ras1* flies. Drugs were fed orally mixed in the animals' food, the screen was performed in duplicate, and potential hits were confirmed in a larger scale format.

Eight hits were identified from this screen (Fig. 2B). Interestingly five of the hits are DNA analogs, three of which are used as chemotherapeutics including capecitabine (5-fluorouracil prodrug), decitabine (cytidine analog used to treat acute myeloid leukemia), and cladrabine (purine analog used to treat hairy cell leukemia). The remaining two DNA analogs were aciclovir and its prodrug valaciclovir, which are guanosine analog antiviral drugs. The antioxidant dexrazoxane was also a weak hit. These provide validation that clinic-relevant hits can be identified in our screening setup.

Two pathway inhibitor drugs were identified. The targeted cancer therapeutic trametinib is a highly specific MEK inhibitor approved for metastatic melanoma. Fluvastatin is an HMG-CoA reductase inhibitor from the cholesterol lowering statin family. Oral administration of trametinib at 1 μM significantly rescued *btl>Ras1* and *btl>Ras1,PTENi* pupal lethality at 25°C (Fig. 2C,D) and larval lethality at 29°C (Fig. 2E,F). 50 μM fluvastatin directed a mild rescue of larval lethality in both genotypes (Fig. 2E,F) but was ineffective in the more stringent pupal lethality assay (Fig. 2C,D). Along with radiation therapy, targeted therapies as stand-alone or adjuvant can yield positive outcomes in lung cancer patients. We therefore focused on the targeted therapeutic drugs trametinib and fluvastatin.

Trametinib and fluvastatin synergized to rescue cancer-like phenotypes

Combining 50 μM fluvastatin with 0.5 μM trametinib significantly enhanced rescue of pupal lethality for both genotypes (Fig. 2C,D) compared to oral administration of trametinib alone.

Further, combining 50 μM fluvastatin with 1 μM trametinib also significantly enhanced rescue of pupal lethality in *btl>Ras1,PTENi* (Fig. 2D) though not *btl>Ras1* (Fig. 2C) compared to 1 μM trametinib alone. Combining fluvastatin with trametinib did not enhance rescue of larval lethality for either genotype (Fig. 2E,F). These data indicate that trametinib is a strong inhibitor of Ras1-based lethality and fluvastatin is a weaker inhibitor. Combining specific concentrations of fluvastatin with trametinib yielded synergistic behavior in promoting adult viability that is more robust in *btl>Ras1,PTENi* than *btl>Ras1* alone. Given the potential clinical relevance of this two drug combination, we further explored their ability to synergize.

In the absence of drug, *btl>Ras1,PTENi* L3 larvae displayed thickened tracheal tubes and ectopic fine terminal branching (Fig. 1C). Oral administration of 1 μM trametinib nearly completely suppressed *btl>Ras1,PTENi* tracheal phenotypes. Specifically, *btl>Ras1,PTENi* animals treated with trametinib did not exhibit the increased terminal branching phenotype observed in DMSO fed control animals nor did tracheal cells display the ‘bulging’ nuclei that contributed to tracheal thickening (Fig. 3B,C; Fig. S1).

We did not observe overproliferation or multilayering within the majority of the *btl>Ras1,PTENi* tracheal system. The cells that make up the larval trachea are polyploid (S Makino, Niiyama, and Asana 1938; Sajiro Makino and Sajiro 1938; Edgar and Orr-Weaver 2001) and are thought to be terminally differentiated. Primary dorsal branches within the L3 larva's second tracheal metamere, however, displayed ectopic cells compared to controls (Fig. S2); this region is populated by dividing imaginal tracheoblasts (Guha and Kornberg 2005). The second tracheal metamere is the source of mitotically active imaginal tracheoblasts (IT) that are used to repopulate the tracheal system during the larval to pupal transition. The second tracheal metamere is bound to the larval wing disc via a transverse connective tracheal branch, which also connects the wing disc to a specialized tracheal structure called the ‘air sac precursor’ (ASP). The ASP is the larval precursor to the large adult dorsal air sacs and provides a readily visualized assay. At the L3 stage of larval development the ASP forms from a small population of mitotically active cells (Sato and Kornberg 2002), proliferating and migrating towards a localized signal of FGF in the dorsal notum region of the wing disc (Sato and Kornberg 2002). During the animal's transition from larva to pupa the majority of larval tracheal cells will histolyze; the pupal trachea is repopulated from imaginal cells similar to those that form the ASP (Yin and Thummel 2005).

btl>Ras1,PTENi animals displayed a range of ASP phenotypes (Fig. 3D-G). 42% of dissected *btl>Ras1,PTENi* wing discs lacked ASPs and 19% were small or abnormally shaped (Fig. 3G), suggesting that these ASPs failed to form properly. 39% of *btl>Ras1,PTENi* ASPs were enlarged; some were significantly overgrown and filled the dorsal region of the wing disc while others displayed milder overgrowth phenotypes (Fig. 3E, 3F). 0.5 μM trametinib reduced the percentage of animals with absent ASPs to 23% compared to 42% in control animals fed DMSO. 50 μM fluvastatin also led to a mild rescue of ASP loss (31%).

Combining trametinib plus fluvastatin decreased the percentage of absent ASPs to 17% (Fig. 3I) and greatly increased the percentage of normal ASPs to 32% compared to fluvastatin (6%) or trametinib (0%) alone (Fig. 3I). We observed no strongly overgrown ASPs in animals fed the two-drug combination (Fig. 3I). Control *btl>Ras1,PTENi* animals fed DMSO had ASPs that comprised 15% of total wing disc size (Fig. 3J). Fluvastatin and trametinib lowered ASP volumes to 11% and 8% respectively. Combining the two drugs further rescued ASP size to 6%, similar to control levels of 4% (Fig. 3J).

The ASP matures into dorsal air sacs that are visible in late pupae within the dorsal thorax (Fig. 3K). Air sacs in the head formed from dilations of the larval cervical trachea are also visible (Fig. 3K). Most *btl>Ras1* and *btl>Ras1,PTENi* pupae displayed a loss of these air sacs (Fig. 3L,M), consistent with the absence of ASPs observed in larval stages; overall, only 20% retained intact dorsal air sacs. This number was strongly improved to 75% in trametinib-fed animals (Fig. 3O,P,Q), consistent with trametinib's rescue of larval ASP loss. We also noted ectopic, GFP-positive tumor-like structures present in the abdominal regions of *btl>Ras1* and *btl>Ras1,PTENi* pupae (Fig. 3L,M). During metamorphosis, most larval tissue including the tracheal epithelium histolyze and are replaced by imaginal tissue (Djabrayan et al. 2014; Cabernard and Affolter 2005; Sato and Kornberg 2002). These GFP-positive abdominal tumor-like foci likely derive from regions that failed to histolyze properly (Fig. 3R,U); alternatively, they may represent migrating cells from larval tracheal areas such as the ASP, which contains cells that endogenously express MMP-1 and migrate across the wing disc. Trametinib consistently reduced the levels of *btl>Ras1,PTENi* GFP-positive abdominal foci (Fig. 3V n=60). Fluvastatin alone had no effect, and combining fluvastatin with trametinib did not lead to further reduction (data not shown), presumably due to the already high level of rescue by trametinib alone (Fig. 3Q).

btl>Ras1,PTENi abdominal ‘tumors’ expressed the cancer biomarker MMP1 (Fig. 3S). MMP1 is often associated with metastasis (Kessenbrock, Plaks, and Werb 2010), and we used time lapse movies to determine if *btl>Ras1,PTENi* abdominal tumors showed migration. GFP positive cells were observed to migrate significant distances in *btl>Ras1,PTENi* pupae (Supplemental Movie); similarly migrating cells were not observed in controls with the caveat that the tracheal system is dynamically reconstructing at this stage and control pupae did not display GFP at strong enough levels to serve as a fully useful comparison.

Fluvastatin reduced trametinib's IC50 in human lung cancer cells

To determine if they exhibited similar synergy in a standard human lung cancer model, the effects of trametinib and fluvastatin were examined in A549 cells, a human lung adenocarcinoma cell line that contains the activated Ras isoform $KRAS^{G12S}$. Dose response curves of trametinib (Fig. 4A) and fluvastatin (Fig. 4A) identified each drug's IC50 as 31.68 nM and 5358 nM respectively. Trametinib dose response curves were then repeated with fixed doses of 1000 to 4000 nM fluvastatin, below its IC50 of 5358 nM (Fig. 4A). Combining fluvastatin with trametinib consistently lowered trametinib's IC50 (Fig. 4B). Using the Chou-Talalay method to calculate combination index (see Experimental Procedures), we determined that lower doses of fluvastatin (1000-3000 nM) exhibited

statistical synergy with trametinib (Fig. 4B). With this data validating the drug combination across platforms, we next explored their mechanisms of action in a whole animal setting.

Inhibition of HMG-CoA reductase and protein prenylation rescued Ras1 driven lethality

Fluvastatin is a member of a large family of 'statin' drugs that inhibit HMG-CoA reductase, an activity that has proven useful clinically for lowering cholesterol (Fig. 5A). Two additional statins, atorvastatin and simvastatin, rescued larval lethality of *btl>Ras1* at 29°C at levels comparable to fluvastatin (Fig. 5B). Most invertebrates including *Drosophila* do not synthesize cholesterol. They rely on dietary sources of cholesterol, indicating that the cholesterol lowering action of statins is not their mechanism of action. Another important function of the HMG-CoA reductase pathway is to synthesize the isoprenoid chains geranylgeranyl pyrophosphate and farnesyl pyrophosphate (Fig. 5A). These are substrates that are added post-translationally to a variety of proteins—including small GTPases such as Ras—in a process known as prenylation. Prenylation facilitates attachment to the cell membrane and activation of proteins including Ras. We blocked prenylation in *btl>Ras1* and *btl>Ras1,PTENi* flies with oral administration of a geranylgeranyl transferase inhibitor (GGTI) and a farnesyl transferase inhibitor (FTI). The GGTI significantly rescued larval lethality of both *btl>Ras1* and *btl>Ras1,PTENi* at 29°C (Fig. 5C,D) similar to fluvastatin, and showed synergy with trametinib (Fig. 5E,F). FTI had no effect (Fig. 5C,D). These results are consistent with results observed when combining trametinib and fluvastatin, further supporting the view that fluvastatin rescues lethality by inhibiting production of isoprenoids such as geranylgeranyl downstream of HMGCR.

Both *btl>Ras1* and *btl>Ras1,PTENi* displayed elevated levels of activated, phosphorylated ERK (pERK) on western blots of dissected L3 tracheal tissue, highlighting activation of the Ras signal transduction pathway (Fig. 6A). As anticipated, trachea from animals fed 1 μM trametinib had strongly reduced levels of pERK, below DMSO controls (Fig. 6C). Phosphorylation of the PI3K pathway effector AKT was strongly elevated in *btl>Ras1,PTENi*, confirming the pathway is also activated (Fig. 6A,B). While trametinib had no effect on pAKT, fluvastatin strongly inhibited pAKT elevation in *btl>Ras1,PTENi* trachea indicating that it acted on PI3K pathway activity (Fig. 6B,D); fluvastatin also showed mild rescue of pERK in *btl>Ras1,PTENi*, but not *btl>Ras1* trachea (Fig. 6C).

These data suggest that fluvastatin acts to rescue lethality by at least two mechanisms. Its ability to act by inhibiting PI3K signaling is consistent with previous mammalian studies (*e.g.*, (Chu, Jia, and Yang 2006; Li and De Souza 2011; Son et al. 2007)). The ability of fluvastatin to also rescue lethality caused by Ras1 alone—which did not show elevated levels of pAKT—indicates that fluvastatin acts through multiple mechanisms; our inhibitor studies indicate that this includes fluvastatin's ability to block protein prenylation.

Fluvastatin rescued drug-mediated whole animal toxicity

While up to 1 μM trametinib rescued our transgenic models, higher doses led to reduced eclosion (emergence of adults): 2 μM trametinib led to poor survival in both cancer models and controls that we attributed to whole animal toxicity. However, combining 50 μM fluvastatin with 2 μM trametinib still led to rescue of *btl>Ras1,PTENi* pupal lethality (Fig.

7A). Feeding 2 μM trametinib to non-transgenic ($y^{-}w^{-}$) flies led to a reduced eclosion rate of 23% compared to 86% of control animals fed DMSO, indicating significant whole animal toxicity. Combining 100 μM fluvastatin with 2 μM trametinib increased eclosion rate to 57% (Fig. 7A). These data indicate that a key aspect of fluvastatin's synergy with trametinib is its ability to reduce the latter's whole body toxicity profile. Surprisingly, fluvastatin was also able to rescue toxic doses of four other drugs: the proteasome inhibitor bortezomib and three mTOR inhibitors (everolimus, rapamycin, and temserolimus; Fig. 7A).

To understand how fluvastatin reduced drug toxicity, we focused on its activity against HMG-CoA reductase. Reducing enzyme activity by introducing the mutation *hmgcr*^{m102023} or (confirmed hypomorph) *hmgcr*^{011522} (Santos and Lehmann 2004) protected animals from toxicity due to high levels of trametinib or everolimus (Fig. 7B,C). Exploring further downstream (Fig. 5A), we reduced activity of Drosophila orthologs of Farnesyl Pyrophosphate Synthase (FPPS) and geranylgeranyl diphosphate synthase (GGPS) and examined toxic levels of trametinib or everolimus. The FPPS mutant *fpps*^{k03514}, previously demonstrated to decrease levels of Rho prenylation (Cook et al. 2012), was strongly insensitive to trametinib toxicity and mildly insensitive to everolimus toxicity (Fig. 7B,C). The null allele *ggps1*$^{qm\text{-}L14.4}$ (Santos and Lehmann 2004) mildly rescued everolimus toxicity (not significant) and had no effect on trametinib toxicity (data not shown). We conclude that, in addition to its anti-tumor effects, fluvastatin can act to reduce whole body toxicity of specific targeted therapeutics to improve overall therapeutic outcome.

Discussion

A whole animal drug screen

We have designed a Drosophila transgenic model that provides a whole animal, genetic platform for exploring lung cancer. Pairing targeted activation of Ras1 with loss of PTEN activity (*btl>Ras1,PTENi*) led to a variety of tracheal defects. Lethality was then used as a quantitative readout to screen a library of 1192 FDA approved drugs for the ability to improve overall animal survival. Several hits were known anti-cancer drugs including DNA analogs that presumably act to decrease overproliferation, validating our approach. Our screen also identified a synergistic relationship between the MEK inhibitor trametinib and the HMG-CoA reductase inhibitor fluvastatin.

Our Drosophila model is not a precise mimic of lung adenocarcinoma but it contains important similarities that indicate it can be a useful one. Pairing oncogenic Ras1 with a knockdown of PTEN within the trachea resulted in overproliferation of larval tissue, loss of pupal air sacs, and generation of tumor-like growths in the pupal abdomen. All phenotypes were strongly rescued by trametinib and by trametinib/fluvastatin combinations. Low dose fluvastatin significantly lowered the IC50 of trametinib in inhibiting growth of the Ras1^{G12V} positive A549 lung adenocarcinoma cell line, demonstrating that fluvastatin acts in part by optimizing trametinib activity within transformed cells. Importantly, the whole animal aspect of the models also allowed us to distinguish between drug combinations that are therapeutic to the animal as opposed to solely killing cancer cells. This advantage was exploited to determine that—in addition to reducing effects of Ras/PTEN on tracheal integrity—

fluvastatin rescued whole animal toxicity associated with trametinib independent of its effects on transformed cells.

Trametinib/fluvastatin synergy

Our results show that, as anticipated, the MEK inhibitor trametinib blocked the rise in pERK associated with overexpression of oncogenic Ras. This is consistent with recent work Mohammed et al. 2012; Miraglia, Högberg, and Stenius 2012; Mistafa and Stenius 2009), statins reduced PI3K pathway activity in Drosophila as assessed by reduced phosphorylation of AKT. Though the mechanism underlying statins' role in inhibiting PI3K signaling is not well understood, they may disrupt protein-protein interactions such as KRAS/PI3K (Chen et al. 2013). 50 μM demonstrating that trametinib acts in Drosophila to reduce Ras pathway activity (Slack et al. 2015). Also consistent with mammalian *in vitro* and *in vivo* data (Y. H. Park et al. 2013; fluvastatin combined with 1 μM trametinib had a significant effect on *btl>Ras1,PTENi* lethality compared to no change in *btl>Ras1* alone (Fig. 2C,D). This is consistent with fluvastatin's effects on Pi3K signaling. Fluvastatin was not able to consistently enhance trametinib's ability to rescue lethality across all drug concentrations, genotypes and temperatures. For example, fluvastatin failed to enhance trametinib-based rescue of larval lethality at 29°C (Fig. 2E,F), possibly reflecting the additional time available to act or differences in larval *vs.* pupal structures.

Statins are traditionally used as cholesterol lowering drugs. However, Drosophila do not synthesize their own cholesterol (Santos and Lehmann 2004) indicating that this is not the mechanism by which fluvastatin is acting to reduce Ras and PI3K pathway activity. Rather, our data is consistent with the view that the anti-cancer activity of statins is due to their ability to inhibit the synthesis of the downstream isoprenoids farnesyl pyrophosphate (FPP) and geranylgeranyl pyrophosphate (GGPP). Protein prenylation creates a lipidated hydrophobic domain that mediates membrane attachment and protein:protein interactions. Prenylation by FPP and GGPP are critical for post-translational modification of Ras and RhoA proteins, respectively (Mo and Elson 2004) and inhibiting geranylgeranyl transferase rescued lethality in our Drosophila lung cancer models. In mammalian systems, inhibition of Rho protein geranylgeranylation (rather than farnesylation of Ras) is likely an important aspect of the anti-cancer effects of statins (Mo and Elson 2004; Konstantinopoulos, Karamouzis, and Papavassiliou 2007; Wong et al. 2002), consistent with our Drosophila data.

Fluvastatin reduced whole animal toxicity

A key discovery of this work is the ability of fluvastatin to reduce whole animal toxicity of multiple targeted drugs independent of its anti-cancer activity. Trametinib is a relatively potent drug including in our cancer models, rescuing lethality at 1 μM food concentration; most effective targeted therapies were optimal within the 100-200 μM range (data not shown). However, trametinib's efficacy was limited by a narrow therapeutic window: 2 μM was toxic to both our cancer model and also wild type animals. This is consistent with a well described toxic profile of trametinib, which includes rashing, gastrointestinal problems, anemia, lymphedema, hypertension, and vascular hemorrhaging, and its use for NSCLC has been limited due to toxicity (Stinchcombe and Johnson 2014).

Here we demonstrate that trametinib's toxicity was reduced by fluvastatin. The detailed mechanism behind fluvastatin's ability to rescue trametinib toxicity is not entirely clear. One clue comes from our observation that other targeted therapeutics were similarly rescued by fluvastatin. Fluvastatin rescued the toxicity of the mTOR inhibitors rapamycin, temserolimus and everolimus. Inhibition of mTORC1 relieves proteasomal degradation of IRS-1 that results in increased PI3K signaling (Carracedo, Baselga, and Pandolfi 2008; O'Reilly et al. 2006; Sun et al. 2005). This suggests that fluvastatin rescues toxicity associated with mTOR inhibition by blocking feedback by activated PI3K signaling, perhaps ‘re-balancing’ Ras/PI3K signaling through the body.

Fluvastatin also rescued the toxicity of the proteasome inhibitor bortezomib. Recent work in our lab suggests that bortezomib can alter PI3K signaling pathway (E. Bangi, unpublished data). Other studies have shown that MEK inhibition leads to increased AKT activation by a negative MEK-EGFR-PI3K feedback loop (Faber et al. 2009; Yoon et al. 2009; Hoeflich et al. 2009; Mirzoeva et al. 2009), again consistent with the view that balanced Ras/PI3K signaling is required for whole body homeostasis. The broad inhibitory nature of statins, due to protein prenylation inhibition, may explain why fluvastatin works well in combination with MEK and PI3K inhibition both directly on cancer cells and in rescuing systemic toxicity. Further studies will be required to determine if statins show a similar role in improving the therapeutic indices of targeted therapies in patients.

Experimental Procedures

Drosophila genotypes used

y^{-};*w*^{1118}, *btl-Gal4* (DGRC -109128), *hmgcr*^{01152} (BL-11522), *hmgcr*^{M102023} (BL-34720), *fpps*^{K03514} (BL-10532), *ggpps*$^{qm\text{-}L14.4}$ (BL-5828)

In vitro assembly of multi-UAS vectors

Drosophila genomic DNA from transgenic flies was used to isolate UAS-GFP, UAS-Dicer1 and UAS-Ras1^{G12V}. A vector from the Vienna Drosophila Resource Center (VDRC) was used to isolate UAS-PTEN-RNAi (VDRC-35731). The following oligos were used to add SpeI and AvrII sites to the 5’ and 3’ ends respectively:

5’-cgcactagttccgtggggtttgaattaac-3’

5’-cgccctaggacggcgatatttctgtggac-3’

AvrII was added to the multicloning region of attB-P[acman]-CmR (DGRC-1244). AvrII/SpeI digested PCR amplified UAS-elements were then ligated into the Pacman vector's AvrII site in the following order: UAS-GFP,UAS-Dicer1,UAS-dRas^{G12V},UAS-PTEN-RNAi in four rounds of cloning. Three vectors (control, Ras1 and Ras1,PTENi) were used to create transgenic lines at the attP 3L-6435776 location (Bloomington #24871).

Drug studies

The Selleck FDA-approved library (catalog #L1300) was dissolved in DMSO buffer to a 100 mM concentration. A PerkinElmer JANUS automated liquid handler was used to create

1.2ml 96 well plates (Abgene catalog #Ab-1068) containing 300μl fly food and 0.3μl drug per well. Drug was added to molten (~50°C)-enriched fly food and then left to solidify at room temperature to yield 96 well plates of food with 100 μM drug and a DMSO concentration of 0.1%. *btl>Ras1,PTENi* embryos were suspended in a solution of 10% glycerol, 1% BSA and 0.1% Tween-20. 5-10μl of this slurry was added to each well at a concentration of ~20 embryos. 96 well plates covered with a breathable membrane (Sigma catalog #Z763624) were placed at 29°C and were scored for the presence of pupae. Positive hits were examined by allowing flies of the indicated genotype to lay 30-60 embryos in 12×75mm, 5ml test tubes (Sarstedt catalog #B00471) containing 1ml of food/drug at the indicated temperature. All inhibitors were from Selleck except the Farnesyltransferase inhibitor (Enzo catalog #G242), and geranylgeranyltransferase inhibitor (Sigma catalog #G5169).

Histology

For larval trachea and ASP analysis, third-instar trachea or wing discs were fixed in 4% paraformaldehyde. For whole larvae air sac analysis late stage pupae (~48 hr after pupae formation [APF]) were collected and the pupal casing was removed prior to imaging. For dissected pupal immunohistochemistry, pupae (~48 hr APF) were frozen in dry ice and then bisected along the anterior-posterior axis, fixed in 4% paraformaldehyde, blocked in 5% BSA PBS-Triton 0.3%. Antibodies used were directed against MMP1 (Developmental Studies Hybridoma Bank catalog #3B8D12) and phosphorylated SRC (Invitrogen catalog #44660G). AlexaFluor secondary antibodies were used. Confocal imaging used a Leica DM5500 Q microscope and image analysis was performed using Adobe Photoshop. ASP and wing disc size were measured by pixel counts using Photoshop histogram.

Western Blots

Trachea from 60 third instar larvae were dissolved in lysis buffer (50mM Tris, 150mM NaCl, 1% Triton X-100, 1mM EDTA) supplemented with protease-inhibitor cocktail and phosphatase-inhibitor cocktail (Sigma). Total protein was quantified using BIORAD protein assay. Samples were boiled, resolved on SDS-PAGE and transferred by standard protocols. Antibodies used were from Cell Signaling except ERK (a gift from L. Zipursky) and syntaxin (DSHB). ImageJ software was used for quantification.

MTT assays using A549 cancer line

A549 cell line was cultured in DMEM buffer supplemented with 10% BSA and a penicillin and streptomycin antibiotics mix. Cells were grown in 75cm^2 sterile polystyrene culture flasks to 80% confluency, trypsinized and re-seeded in equal aliquots into 96-well plates. After 2 days and ~50 confluency, media was removed and replaced with DMSO or drug containing media. Cells were allowed to grow for another 6 days, after which the thiazolyl blue tetrazolium bromide (MTT) assay was performed. Cell media was removed and replaced with MTT-containing media (1 mg ml^{-1} final concentration) and cells were allowed to grow at 37 °C for another 3.5 h. MTT media was removed and MTT precipitate dissolved in 4 mM HCl, 0.1% NP40 in isopropanol, solvent by shaking for 1 h. Spectrophotometric readings at 590 nm and 630 nm using a 96-well-plate reader were used to establish growth

and viability of cells. Each drug dose was tested in quadruplicates and experiments repeated in triplicate.

Combination index (CI) was determined using the formula outlined by the theorem of Chou-Talalay: CI = ([Tra]c / [Tra]) + ([Flu]c / [Flu]) + ([Tra]c X [Flu]c / [Tra] X [Flu]) [Tra] and [Flu] are IC50 values of the drugs alone; [Tra]c and [Flu]c are IC50 values of the drugs in combination. CI values were used to determine synergy (CI < 0.9), additivity (0.9 < CI < 1.1), and antagonism (CI > 1.1) of the drug combinations tested (Chou and Talalay, 1983; Chou 2010).

Time lapse pupal movies

Late stage (>48 hr APF) pupae were selected, placed on a microscope slide and imaged with a Leica DM5500 Q microscope. 60 ms exposures were taken every 7 minutes. Movie shown is 60 frames (7 hours).

Supplementary Material

Refer to Web version on PubMed Central for supplementary material.

Acknowledgements

We thank members of the Cagan laboratory for technical assistance and for helpful discussions. We thank Vienna Drosophila Resource Center and the Bloomington Drosophila Stock Center for Drosophila reagents. Microscopy was performed in part at the Microscopy Shared Resource Facility at the Icahn School of Medicine at Mount Sinai. This research was supported by National Institutes of Health grants R01-CA170495, R01-CA170495 and R01-CA109730, Department of Defense grant W81XWH-15-1-0111 and a grant from the Lung Cancer Research Foundation.

References

Andrew, Deborah J.; Ewald, Andrew J. Morphogenesis of Epithelial Tubes: Insights into Tube Formation, Elongation, and Elaboration. Developmental Biology. 2010; 341(1):34–55. [PubMed: 19778532]

Behr, Matthias. Molecular Aspects of Respiratory and Vascular Tube Development. Respiratory Physiology & Neurobiology. Aug; 2010 173(Suppl):S33–6. [PubMed: 20403463]

Bellusci S, Furuta Y, Rush MG, Henderson R, Winnier G, Hogan BL. Involvement of Sonic Hedgehog (Shh) in Mouse Embryonic Lung Growth and Morphogenesis. Development. 1997; 124(1):53–63. [PubMed: 9006067]

Cabernard, Clemens; Affolter, Markus. Distinct Roles for Two Receptor Tyrosine Kinases in Epithelial Branching Morphogenesis in Drosophila. Developmental Cell. 2005; 9(6):831–42. [PubMed: 16326394]

Cancer Genome Atlas Research Network. Comprehensive Genomic Characterization of Squamous Cell Lung Cancers. Nature. 2012; 489(7417):519–25. [PubMed: 22960745]

Carracedo, Arkaitz; Baselga, Jose; Paolo Pandolfi, Pier. Deconstructing Feedback-Signaling Networks to Improve Anticancer Therapy with mTORC1 Inhibitors. Cell Cycle. 2008; 7(24):3805–9. [PubMed: 19098454]

Chen J, Bi H, Hou J, Zhang X, Zhang C, Yue L, Wen X, et al. Atorvastatin Overcomes Gefitinib Resistance in KRAS Mutant Human Non-Small Cell Lung Carcinoma Cells. Cell Death & Disease. Sep.2013 4:e814. [PubMed: 24071646]

Chou, Ting-Chao. Drug Combination Studies and Their Synergy Quantification Using the Chou-Talalay Method. Cancer Research. 2010; 70(2):440–446. [PubMed: 20068163]

Chou, Ting-Chao; Talalay, P. Analysis of Combined Drug Effects: A New Look at a Very Old Problem. Trends in Pharmacological Sciences. 1983; 4:450–454.

Chu, Guili; Jia, Ruhan; Yang, Dingping. Fluvastatin Prevents Oxidized Low-Density Lipoprotein-Induced Injury of Renal Tubular Epithelial Cells by Inhibiting the Phosphatidylinositol 3-kinase/Akt-Signaling Pathway. Journal of Nephrology. 2006; 19(3):286–95. [PubMed: 16874687]

Cook, Mandy; Mani, Priya; Wentzell, Jill S.; Kretzschmar, Doris. Increased RhoA Prenylation in the Loechrig (loe) Mutant Leads to Progressive Neurodegeneration. PloS One. 2012; 7(9):e44440. [PubMed: 22970217]

Denes, Alexandru S.; Kanca, Oguz; Affolter, Markus. A cellular process that includes asymmetric cytokinesis remodels the dorsal tracheal branches in Drosophila larvae. Development. 2015; 15142(10):1794–805. [PubMed: 25968315]

Djabrayan, Nareg J-V.; Cruz, Josefa; de Miguel, Cristina; Franch-Marro, Xavier; Casanova, Jordi. Specification of Differentiated Adult Progenitors via Inhibition of Endocycle Entry in the Drosophila Trachea. Cell Reports. 2014; 9(3):859–65. [PubMed: 25437542]

Edgar BA, Orr-Weaver TL. Endoreplication Cell Cycles: More for Less. Cell. 2001; 105(3):297–306. [PubMed: 11348589]

Faber, Anthony C.; Li, Danan; Song, Youngchul; Liang, Mei-Chih; Yeap, Beow Y.; Bronson, Roderick T.; Lifshits, Eugene, et al. Differential Induction of Apoptosis in HER2 and EGFR Addicted Cancers Following PI3K Inhibition. Proceedings of the National Academy of Sciences of the United States of America. 2009; 106(46):19503–8. [PubMed: 19850869]

Guha, Arjun; Kornberg, Thomas B. Tracheal Branch Repopulation Precedes Induction of the Drosophila Dorsal Air Sac Primordium. Developmental Biology. 2005; 287(1):192–200. [PubMed: 16198330]

Hoeflich, Klaus P.; O'Brien, Carol; Boyd, Zachary; Cavet, Guy; Guerrero, Steve; Jung, Kenneth; Januario, Tom, et al. In Vivo Antitumor Activity of MEK and Phosphatidylinositol 3-Kinase Inhibitors in Basal-like Breast Cancer Models. Clinical Cancer Research: An Official Journal of the American Association for Cancer Research. 2009; 15(14):4649–64. [PubMed: 19567590]

Kandoth, Cyriac; McLellan, Michael D.; Vandin, Fabio; Ye, Kai; Niu, Beifang; Lu, Charles; Xie, Mingchao, et al. Mutational Landscape and Significance across 12 Major Cancer Types. Nature. 2013; 502(7471):333–39. [PubMed: 24132290]

Kessenbrock, Kai; Plaks, Vicki; Werb, Zena. Matrix Metalloproteinases: Regulators of the Tumor Microenvironment. Cell. 2010; 141(1):52–67. [PubMed: 20371345]

Konstantinopoulos, Panagiotis A.; Karamouzis, Michalis V.; Papavassiliou, Athanasios G. Post-Translational Modifications and Regulation of the RAS Superfamily of GTPases as Anticancer Targets. Nature Reviews. Drug Discovery. 2007; 6(7):541–55. [PubMed: 17585331]

Li, Shaojuan; De Souza, Paul. Ras Isoprenylation and pAkt Inhibition by Zoledronic Acid and Fluvastatin Enhances Paclitaxel Activity in T24 Bladder Cancer Cells. Cancers. 2011; 3(1):662–74. [PubMed: 24212635]

Makino S, Niiyama H, Asana JJ. On the Supernumerary Chromosomes in the Mole-Cricket Gryllotalpa Africana de BEAUVOIS from India (A Preliminary Report). The Japanese Journal of Genetics. 1938; 14(6):272–77.

Makino, Sajiro; Sajiro, Makino. A Morphological Study of the Nucleus in Various Kinds of Somatic Cells of Drosophila Virilis. Cytologia. 1938; 9(2-3):272–82.

Miraglia, Erica; Högberg, Johan; Stenius, Ulla. Statins Exhibit Anticancer Effects through Modifications of the pAkt Signaling Pathway. International Journal of Oncology. 2012; 40(3):867–75. [PubMed: 21994073]

Mirzoeva, Olga K.; Das, Debopriya; Heiser, Laura M.; Bhattacharya, Sanchita; Siwak, Doris; Gendelman, Rina; Bayani, Nora, et al. Basal Subtype and MAPK/ERK Kinase (MEK)-Phosphoinositide 3-Kinase Feedback Signaling Determine Susceptibility of Breast Cancer Cells to MEK Inhibition. Cancer Research. 2009; 69(2):565–72. [PubMed: 19147570]

Mistafa, Oras; Stenius, Ulla. Statins Inhibit Akt/PKB Signaling via P2X7 Receptor in Pancreatic Cancer Cells. Biochemical Pharmacology. 2009; 78(9):1115–26. [PubMed: 19540829]

Mo, Huanbiao; Elson, Charles E. Studies of the Isoprenoid-Mediated Inhibition of Mevalonate Synthesis Applied to Cancer Chemotherapy and Chemoprevention. Experimental Biology and Medicine. 2004; 229(7):567–85. [PubMed: 15229351]

Mohammed, Altaf; Qian, Li; Janakiram, Naveena B.; Lightfoot, Stan; Steele, Vernon E.; Rao, Chinthalapally V. Atorvastatin Delays Progression of Pancreatic Lesions to Carcinoma by Regulating PI3/AKT Signaling in p48Cre/+ LSL-KrasG12D/+ Mice. International Journal of Cancer. Journal International Du Cancer. 2012; 131(8):1951–62. [PubMed: 22287227]

O'Reilly, Kathryn E.; Rojo, Fredi; She, Qing-Bai; Solit, David; Mills, Gordon B.; Smith, Debra; Lane, Heidi, et al. mTOR Inhibition Induces Upstream Receptor Tyrosine Kinase Signaling and Activates Akt. Cancer Research. 2006; 66(3):1500–1508. [PubMed: 16452206]

Park WY, Miranda B, Lebeche D, Hashimoto G, Cardoso WV. FGF-10 Is a Chemotactic Factor for Distal Epithelial Buds during Lung Development. Developmental Biology. 1998; 201(2):125–34. [PubMed: 9740653]

Park, Yeon Hee; Hyun Jung, Hae; Seok Ahn, Jin; Im, Young-Hyuck. Statin Induces Inhibition of Triple Negative Breast Cancer (TNBC) Cells via PI3K Pathway. Biochemical and Biophysical Research Communications. 2013; 439(2):275–79. [PubMed: 23973711]

Roeder, Thomas; Isermann, Kerstin; Kallsen, Kim; Uliczka, Karin; Wagner, Christina. A Drosophila Asthma Model - What the Fly Tells Us about Inflammatory Diseases of the Lung. Advances in Experimental Medicine and Biology. 2012; 710:37–47. [PubMed: 22127884]

Santos, Ana C.; Lehmann, Ruth. Isoprenoids Control Germ Cell Migration Downstream of HMGCoA Reductase. Developmental Cell. 2004; 6(2):283–93. [PubMed: 14960281]

Sato, Makoto; Kornberg, Thomas B. FGF Is an Essential Mitogen and Chemoattractant for the Air Sacs of the Drosophila Tracheal System. Developmental Cell. 2002; 3(2):195–207. [PubMed: 12194851]

Shiga, Yasuhiro; Tanaka-Matakatsu, Miho; Hayashi, Shigeo. A Nuclear GFP/d835-Galactosidase Fusion Protein as a Marker for Morphogenesis in Living Drosophila. Development Growth & Differentiation. 1996; 38:99–106.

Slack, Cathy; Alic, Nazif; Foley, Andrea; Cabecinha, Melissa; Hoddinott, Matthew P.; Partridge, Linda. The Ras-Erk-ETS-Signaling Pathway Is a Drug Target for Longevity. Cell. 2015; 162(1): 72–83. [PubMed: 26119340]

Son, Bo-Kyung; Kozaki, Koichi; Iijima, Katsuya; Eto, Masato; Nakano, Toru; Akishita, Masahiro; Ouchi, Yasuyoshi. Gas6/Axl-PI3K/Akt Pathway Plays a Central Role in the Effect of Statind835s on Inorganic Phosphate-Induced Calcification of Vascular Smooth Muscle Cells. European Journal of Pharmacology. 2007; 556(1-3):1–8. [PubMed: 17196959]

Stinchcombe, Thomas E.; Johnson, Gary L. MEK Inhibition in Non-Small Cell Lung Cancer. Lung Cancer. 2014; 86(2):121–25. [PubMed: 25257766]

Sun, Shi-Yong; Rosenberg, Laura M.; Wang, Xuerong; Zhou, Zhongmei; Yue, Ping; Fu, Haian; Khuri, Fadlo R. Activation of Akt and eIF4E Survival Pathways by Rapamycin-Mediated Mammalian Target of Rapamycin Inhibition. Cancer Research. 2005; 65(16):7052–58. [PubMed: 16103051]

Weaver, Molly; Krasnow, Mark. Dual origin of tissue-specific progenitor cells in Drosophila tracheal remodeling. Science. Sep 12; 2008 321(5895):1496–9. 2008. [PubMed: 18669822]

Wong WWL, Dimitroulakos J, Minden MD, Penn LZ. HMG-CoA Reductase Inhibitors and the Malignant Cell: The Statin Family of Drugs as Triggers of Tumor-Specific Apoptosis. Leukemia. 2002; 16(4):508–19. [PubMed: 11960327]

Yin, Viravuth P.; Thummel, Carl S. Mechanisms of Steroid-Triggered Programmed Cell Death in Drosophila. Seminars in Cell & Developmental Biology. 2005; 16(2):237–43. [PubMed: 15797834]

Yoon, Young-Kwang; Kim, Hwang-Phill; Han, Sae-Won; Hur, Hyung-Seok; Youn Oh, Do; Im, Seock-Ah; Bang, Yung-Jue; Kim, Tae-You. Combination of EGFR and MEK1/2 Inhibitor Shows Synergistic Effects by Suppressing EGFR/HER3-Dependent AKT Activation in Human Gastric Cancer Cells. Molecular Cancer Therapeutics. 2009; 8(9):2526–36. [PubMed: 19755509]

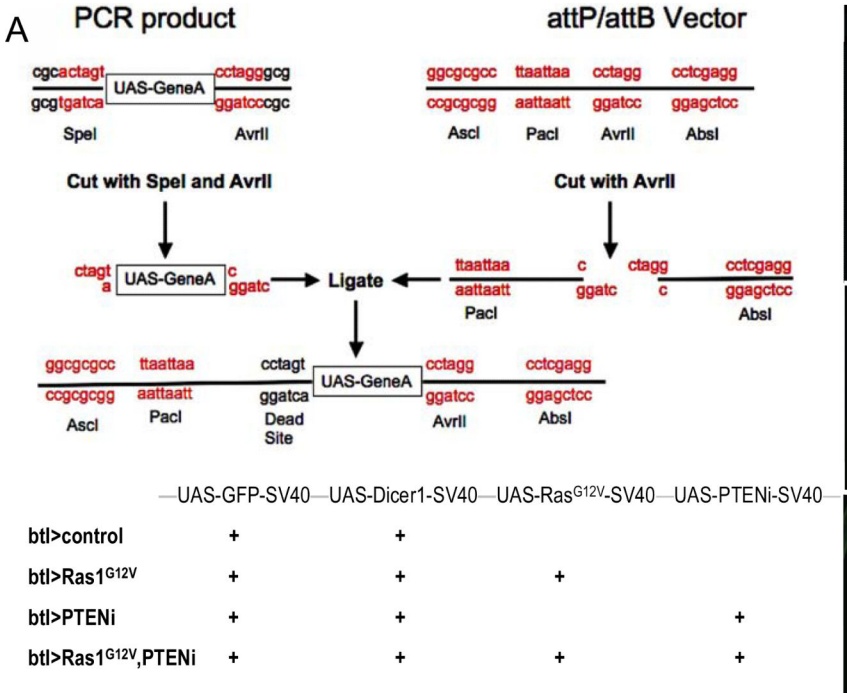

Figure 1. A multigenic Drosophila lung cancer model

(A) Multiple UAS-containing transgenes were combined into vectors using a repeat ligation method. Up to four UAS elements were added to a single vector in the order and orientation shown. The four transgenic lines used in this study are indicated in the lower panel. (B-C"), *btl>Ras1,PTENi* larvae exhibited enlarged and thickened tracheal tubes compared to *btl>control* larvae. Higher magnification views are shown to visualize the enlarged nuclei.

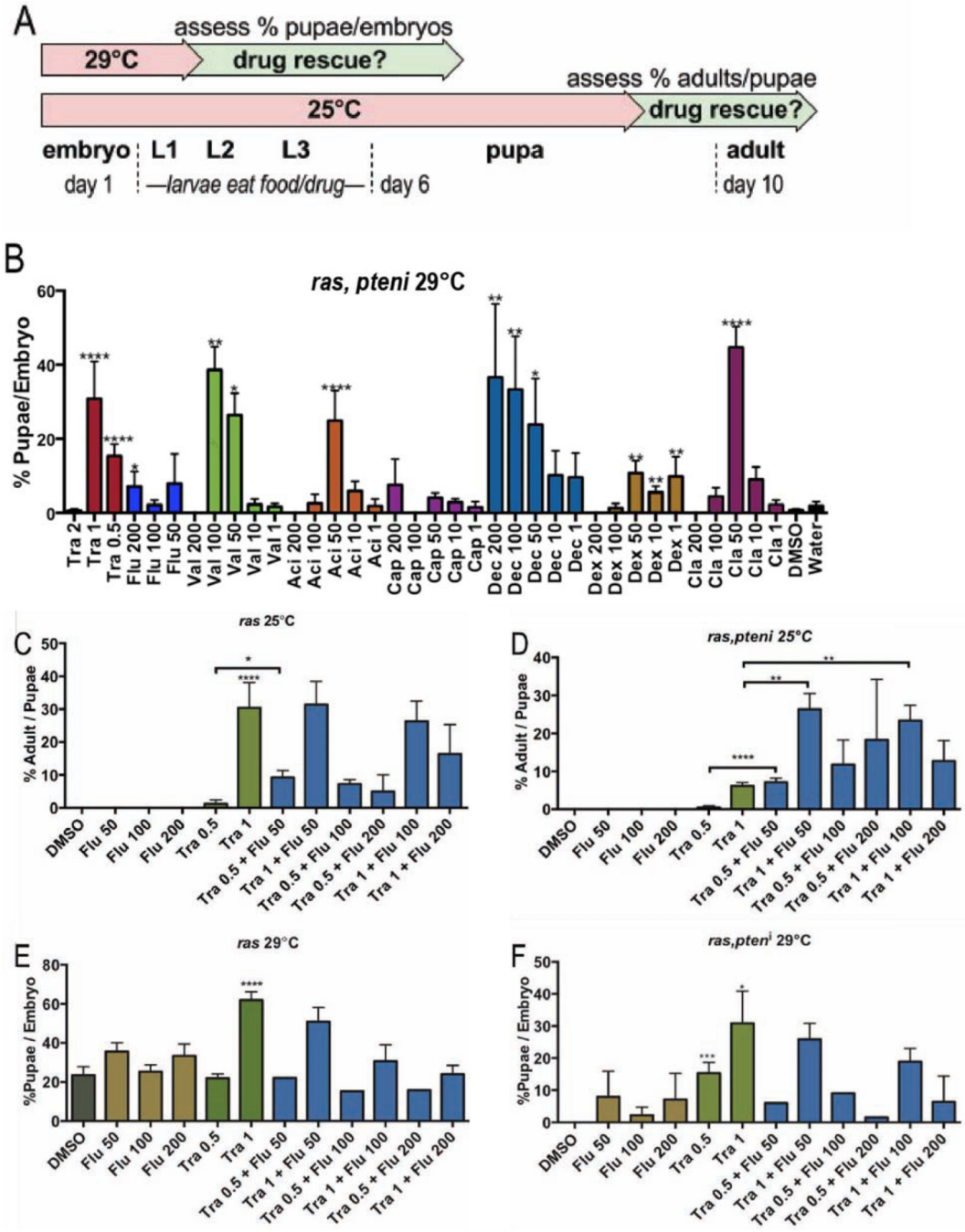

Figure 2. A lethality based large scale drug screen

(A) Flowchart of drug experiments. *btl>Ras1* combinations led to early larval lethality at 29°C and late pupal lethality at 25°C; drug efficacy was determined by measuring the ratio of pupae:embryos at 29°C or adults:pupae at 25°C.

(B) Nine positive hits from an FDA library screen were tested in larger scale format (P values are *≤0.05, **≤0.01, ***≤0.01, ****≤0.0001). All drug concentrations are μM. Tra=trametinib, Flu=fluvastatin, Val=valaciclovir, Aci=aciclovir, Cap=capecitabine, Dec=decitabine, Dex=dexrazoxane and Cla=cladrabine.

(C) 1 μM trametinib rescued *btl>Ras1* pupal lethality ($p \leq 0.0001$) at 25°C. 50 μM fluvastatin + 0.5 μM trametinib rescued more fully than 0.5 μM trametinib alone ($p \leq 0.05$).
(D) 1 μM trametinib rescued *blt>Ras1,PTEN* larval lethality ($p \leq 0.0001$) at 25°C. Fluvastatin synergized with trametinib at select concentrations.
(E) 1 μM trametinib rescued *btl>Ras1,PTENi* pupal lethality ($p \leq 0.0001$) at 29°C; fluvastatin failed to improve rescue.
(F) Trametinib at 0.5 μM ($p \leq 0.01$) and 1 μM ($p \leq 0.05$) rescued *btl>Ras1,PTENi* larval lethality at 29°C; high levels of fluvastatin failed to improve trametinib-based rescue in experiments presented in Figures C-F, presumably due to toxicity at 200 μM.
(Values represent mean ± SEM).

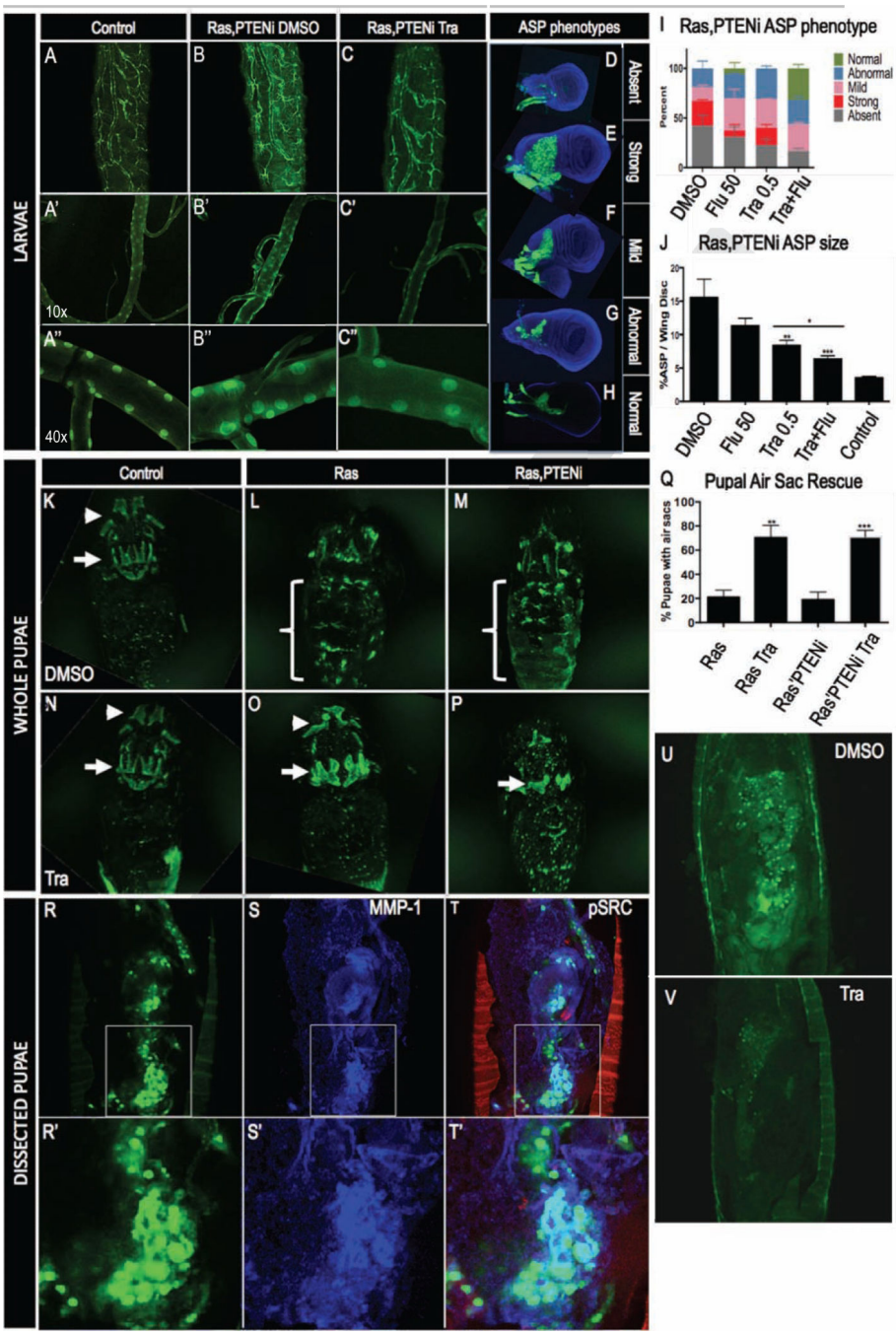

Figure 3. Trametinib and fluvastatin rescue tracheal defects

(A-A") *btl>control* whole larvae (A) and dissected (A'-A") trachea.

(B-B") *btl>Ras1,PTENi* whole larvae have increased fine tracheal branching (B). Dissected *btl>Ras1,PTENi* trachea displayed thickened tracheal tubes and enlarged cell nuclei (B'-B").

(C-C") 1 μM trametinib rescued *blt>Ras1,PTENi* ectopic fine tracheal branches, tracheal thickening and enlarged cell nuclei.

(D-G) *btl>Ras1,PTENi* exhibited multiple alterations in anterior sac precursor (ASP) development including ASP absence (D), strong overproliferation (E), mild overproliferation (F), and abnormal shape (G).
(H) Representative *btl>Ras1,PTENi* ASP rescued by 0.5 μM trametinib + 50 μM fluvastatin.
(I) In *btl>Ras1,PTENi* animals, 0.5 μM trametinib + 50 μM fluvastatin increased percentage of normal ASPs and lowered percentage of absent and strongly overgrown ASP phenotypes compared to either drug alone.
(J) In *btl>Ras1,PTENi* animals, ASPs comprised 15% of wing disc volume compared to 3% in control ASPs. 50 μM fluvastatin mildly and 0.5 μM trametinib significantly ($p \leq 0.01$) rescued ASP overgrowth. Combining both drugs significantly lowered ASP size compared to trametinib alone (bar, $p \leq 0.05$).
(K) Pupal air sacs in whole pupae were visible in *btl>control* animals in the head (arrowhead) and thorax (arrow).
(L,M) *btl>Ras1* or *btl>Ras1,PTENi* animals exhibited loss of pupal air sacs and gain of abdominal tumors (brackets).
(O,P) 1 μM trametinib rescued pupal air sacs and inhibited abdominal tumors in *btl>Ras1* (O) and *btl>Ras1,PTENi* (P) animals.
(Q) Quantification of 1 μM trametinib rescue of *btl>Ras1* ($p \leq 0.01$) and *btl>Ras1,PTENi* ($p \leq 0.001$) tumor formation.
(R-T) Dissected *btl>Ras1,PTENi* pupae had large GFP positive abdominal tumors (R,U) that were MMP1 positive (S). Phosphorylated SRC outlined the pupal casing (T).
(V) 1 μM trametinib consistently rescued formation of pupal abdominal tumors (n=60).
All experiments were performed at 25°C except ASP phenotyping at 27°C.
(Values represent mean ± SEM).

A

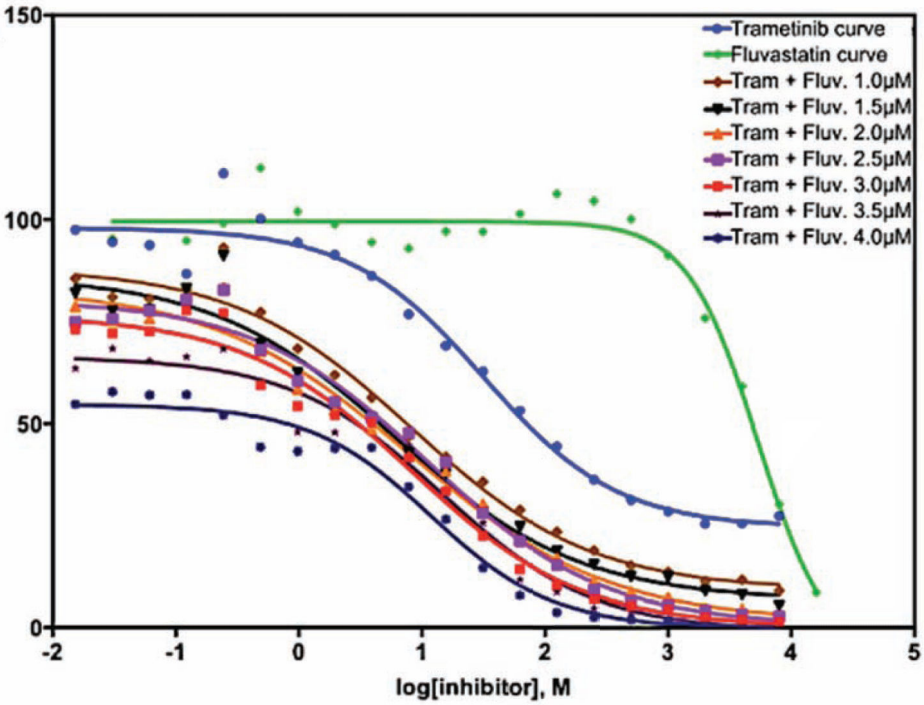

B

Drug	IC50	CI	Result
trametinib curve	31.68		
fluvastatin curve	5358		
tram + fluv. 1000	7.65	0.329	synergy
tram + fluv. 1500	5.87	0.398	synergy
tram + fluv. 2000	8.30	0.552	synergy
tram + fluv. 2500	11.03	0.721	synergy
tram + fluv. 3000	8.19	0.761	synergy
tram + fluv. 3500	13.25	0.997	additive
tram + fluv. 4000	11.73	1.068	additive

Figure 4. Trametinib and fluvastatin synergized to inhibit growth in A549 lung adenocarcinoma cells

(A) Percent viability of A549 cells determined by MTT assay plotted on a logarithmic molar dose curve scale. Shown are trametinib and fluvastatin single drug dose curves and fluvastatin dose curve with fixed trametinib dosing.

(B) IC50 for fluvastatin, trametinib and trametinib plus fluvastatin, calculated with Prism software. The combination index (CI) theorem of Chou-Talalay was used to determine synergy versus additive effects. 1-3 μM fluvastatin lowered the IC50 of trametinib in a synergistic manner.

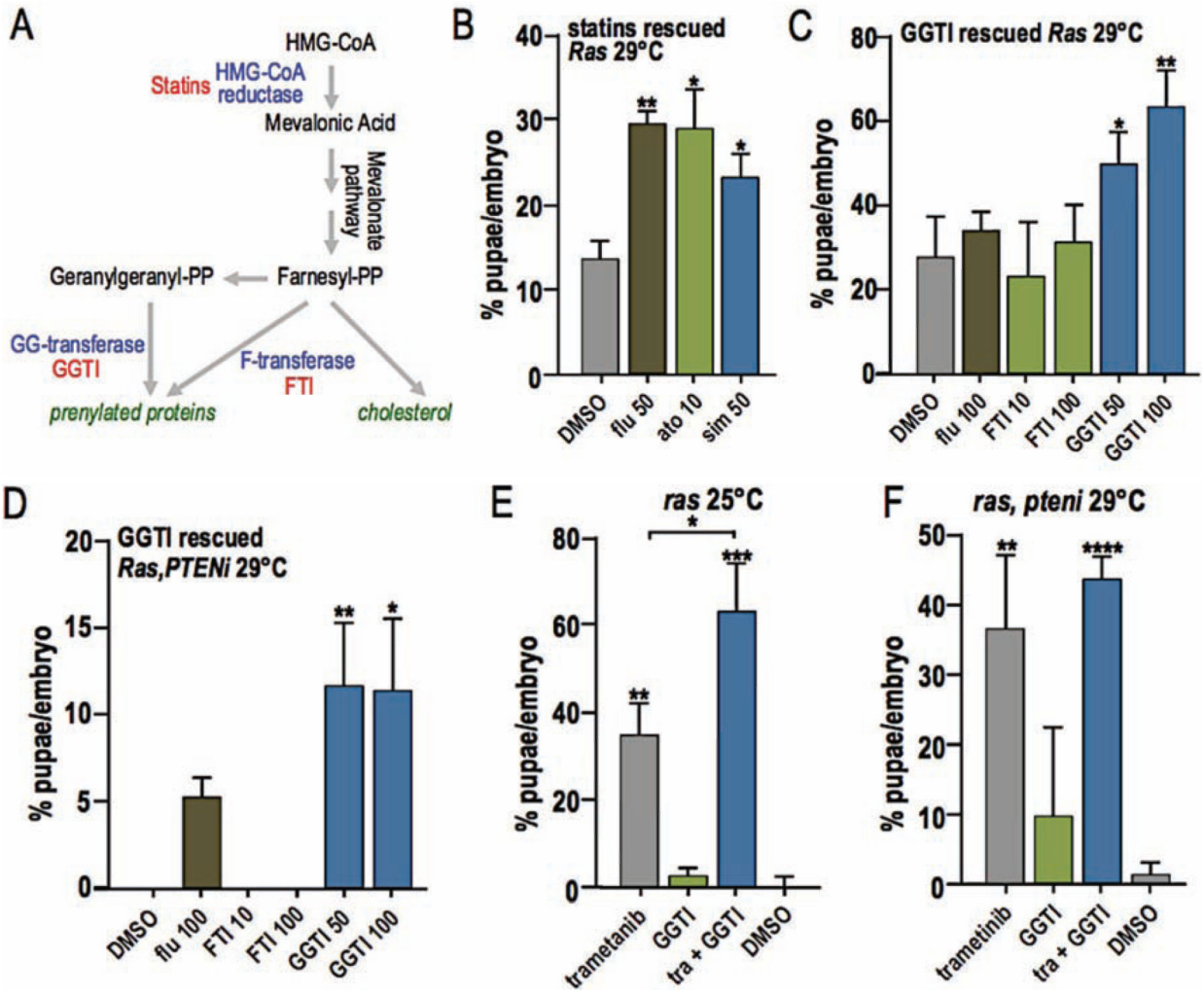

Figure 5. Protein prenylation inhibition rescues Ras1 driven lethality

(A) HMG-CoA pathway. HMG-CoA reductase is the rate limiting enzyme in cholesterol synthesis and is inhibited by statins. The pathway also produces farnesyl-PP and geranylgeranyl-PP, substrates used for protein prenylation. Geranylgeranyl-transferase and farnesyl-transferase, two enzymes used in protein prenylation, are inhibited by GGTI and FTI. Inhibitors listed in red.

(B) Two additional statins, atorvastatin ($p \leq 0.05$) and simvastatin ($p \leq 0.05$), rescued *btl>Ras1* larval lethality in a manner similar to fluvastatin ($p \leq 0.01$).

(C,D) The prenylation inhibitor geranylgeranyl transferase inhibitor (GGTI) rescued lethality directed by *btl>Ras1* (C, 50 μM $p \leq 0.05$, 100 μM $p \leq 0.01$) and *btl>Ras1,PTENi* (D, 50 μM $p \leq 0.01$, 100 μM $p \leq 0.05$).

(E,F) Geranylgeranyl transferase inhibitor (GGTI) combined with trametinib significantly rescued *btl>Ras1*-mediated pupal lethality more strongly than either drug alone (E, 1 μM trametinib + 100 μM GGTI $p \leq 0.05$). Though an apparent trend towards synergy was observed in rescue of *btl>Ras1,PTENi* lethality, the results were not statistically significant (F).

(Values represent mean ± SEM).

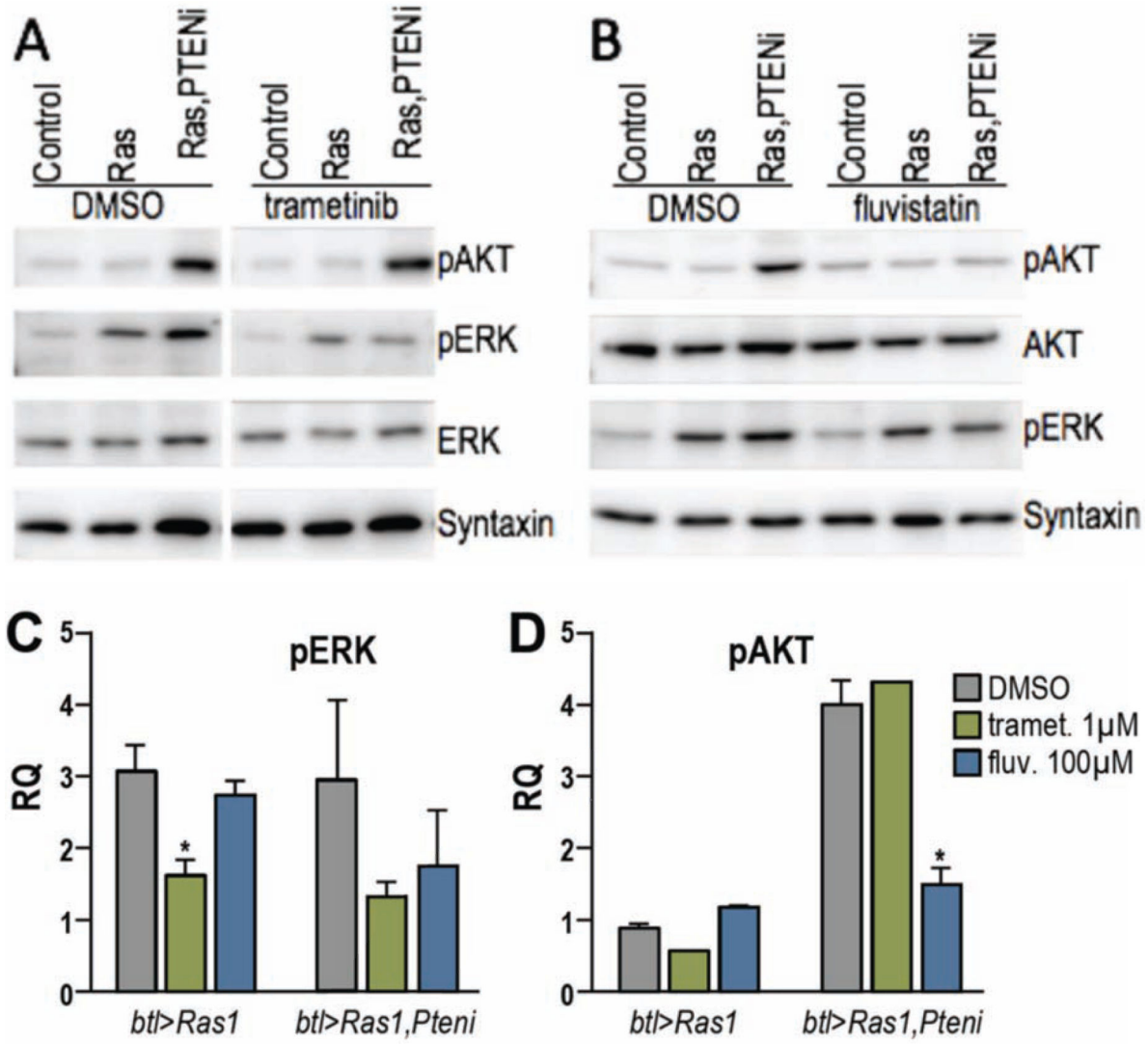

Figure 6. Trametinib reduced pERK, fluvastatin reduced pAKT

Western blots performed on third instar larval tracheal tissue from *btl>Ras1* or *btl>Ras1,PTENi*.

(A) 1 μM trametinib blocked Ras1-dependent, elevated levels of phosphorylated ERK (pERK) but had no effect on phosphorylated AKT (pAKT).

(B) 100 μM fluvastatin reduced a PTEN1-dependent elevation in pAKT.

(C) Quantification of drug effects on pERK levels, which were strongly reduced by trametinib (Ras1 $p \leq 0.05$; Ras1,PTENi $p = 0.2513$) and weakly reduced by fluvastatin (Ras1,PTENi $p = 0.5564$).

(D) Trametinib had no effect on pAKT. Fluvastatin reduced pAKT in *btl>Ras1,PTENi* larvae ($p \leq 0.05$). Values represent mean ± SEM.

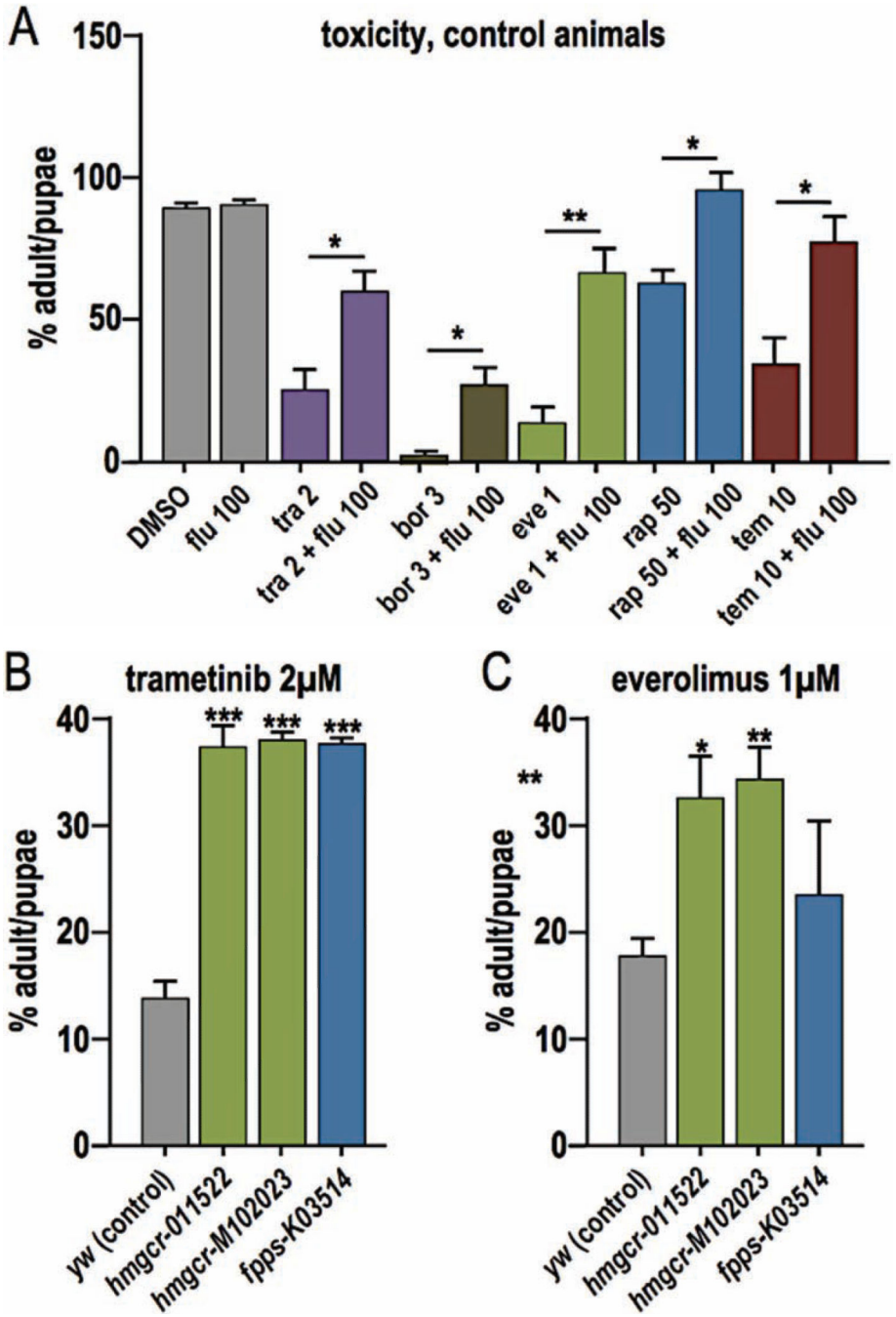

Figure 7. Fluvastatin rescues toxicity caused by other drugs

(A) 2 μM trametinib was toxic to control flies; toxicity was rescued by 50 μM fluvastatin (Flu; $p \leq 0.05$). The proteasome inhibitor bortezomib (bor; $p \leq 0.05$) and three mTOR inhibitors—everolimus (eve; $p \leq 0.01$), rapamycin (rap; $p \leq 0.05$) and temserolimus (tem; $p \leq 0.05$)—were also toxic at the specified doses (μM). All were partially rescued by 50 μM fluvastatin.

(B, C) Mutant lines of the Drosophila homologs of HMG-CoA reductase and farnesyl pyrophosphate synthase were insensitive to trametinib and/or everolimus toxicity.

P values are *≤0.05, **≤0.01, ***≤0.01, ****≤0.0001; values represent mean ± SEM.